Journal of Catalysis 258 (2008) 143–152

Contents lists available at ScienceDirect

Journal of Catalysis

www.elsevier.com/locate/jcat

Electrocatalytic activity and stability of Pt supported on Sb-doped SnO_2 nanoparticles for direct alcohol fuel cells

Kug-Seung Lee, In-Su Park, Yong-Hun Cho, Dae-Sik Jung, Namgee Jung, Hee-Young Park, Yung-Eun Sung *

School of Chemical and Biological Engineering and Research Center for Energy Conversion and Storage, Seoul National University, Seoul 151-744, South Korea

ARTICLE INFO

Article history:
Received 29 November 2007
Revised 17 May 2008
Accepted 4 June 2008
Available online 9 July 2008

Keywords:
Direct alcohol fuel cell
Electrocatalyst
Antimony-doped tin oxide
Ethanol electrooxidation
Methanol electrooxidation
Electrochemical stability
Potential cycling

ABSTRACT

Electrocatalytic activities and stabilities of Pt supported on Sb-doped SnO_2 (ATO) were examined for methanol (MOR) and ethanol (EOR) oxidation reactions. Pt colloidal particles were deposited on ATO nanoparticles (Pt/ATO) with various amounts of Pt loading. The prepared electrocatalysts were characterized by X-ray diffraction, transmission electron microscopy (TEM), X-ray photoelectron spectroscopy, thermogravimetric analysis, and cyclic voltammetry. Electrochemical activities of the Pt/ATO for CO oxidation, MOR, and EOR were compared with those of Pt supported on carbon (Pt/C). The MOR and EOR activities of the Pt/ATO were enhanced over those of the Pt/C with decreasing amounts of Pt loaded on ATO. The Pt/ATO exhibited much higher electrochemical and thermal stabilities than the Pt/C. According to TEM, the growth rate of Pt particles was lower in the Pt/ATO than in the Pt/C. The ATO nanoparticles appear to be promising support materials that promote electrochemical reactions and stabilize catalyst particles in direct alcohol fuel cells.

1. Introduction

There has been much recent interest in the development of electrocatalysts for direct alcohol fuel cells (DAFCs) used in mobile power supply systems. Methanol and ethanol have been used as fuel mainly due to their several advantages: low cost, high theoretical energy density, and ease of use. Up to now, Pt-based electrocatalysts have been considered the most promising electrode materials for electrooxidation of methanol or ethanol [1–6]. These electrocatalysts are composed mainly of nanoparticles and support material. Electrocatalyst particles are deposited on the support material to increase the surface area and reduce sintering effects.

Carbon is a common choice for supporting nanosized electrocatalyst particles in DAFCs because of its large surface area, high electrical conductivity, and pore structures [1,7,8]. However, this inert material (carbon) does not help electrocatalytic activities, but serves only as a mechanical support. A few studies have been reported in this regard, mostly using oxide material as active or promoting support [9–13].

SnO_2 has been proposed as a good candidate for the support material because of its chemical properties: It adsorbs OH species at low potentials or induces the electronic effect with Pt catalysts. These properties promote the electrooxidation of CO and low-molecular-weight alcohol, such as methanol and ethanol [12,14,15].

Aside from its electrochemical activity, the stability of the support material in electrochemical reactions also merits consideration. Carbon has been known to oxidize electrochemically in aqueous solutions by the following reaction [16]:

$$C + 2H_2O \rightarrow CO_2 + 4H^+ + 4e^- \quad (0.207\ \text{V vs SHE, } 25\,^\circ\text{C}). \qquad (1)$$

Pt further accelerates the corrosion rate of carbon, leading to severe agglomeration or growth of electrocatalyst particles and thus degradation of cell performance [17,18]. Conducting oxides have been studied to determine whether they can serve as good corrosion-resistant supports. Ioroi et al. [19] and Chhina et al. [20] investigated the oxidation resistance of supports using titanium oxide and indium tin oxide, respectively. They showed that the oxide materials have much higher corrosion resistance and smaller decreases in active surface area compared with the carbon support.

In the present work, we prepared Pt supported on Sb-doped SnO_2 (Pt/ATO) nanoparticles with various levels of Pt loading on ATO for DAFCs. SnO_2 was doped with Sb to increase its electrical conductivity, because undoped SnO_2 is a poor electrical conductor. The electrochemical activity and stability of the prepared electrocatalysts were investigated. The activities of the Pt/ATO for methanol (MOR) and ethanol (EOR) oxidation reaction were compared with those of Pt supported on carbon (Pt/C) using cyclic voltammetry (CV) and chronoamperometry. The stability of the

* Corresponding author. Fax: +82 2 888 1604.
E-mail address: ysung@snu.ac.kr (Y.-E. Sung).

0021-9517/$ – see front matter
doi:10.1016/j.jcat.2008.06.007

prepared electrocatalysts was studied using potential cycling experiments and thermogravimetric analysis (TGA).

2. Experimental

2.1. Electrocatalyst preparation

All aqueous solutions were made with deionized (DI) water, which was further purified with a Mili-Q system (Millipore water, 18.2 MΩ cm). The $SnCl_4{\cdot}5H_2O$, $SbCl_3$, $H_2PtCl_6{\cdot}xH_2O$, and 37% HCl aqueous solution were obtained from Aldrich. Sodium hydroxide beads (98%) and ethylene glycol (99.5%) were purchased from Samchun Chemicals.

The ATO nanoparticles were synthesized as follows. First, 10.517 g of $SnCl_4{\cdot}5H_2O$, 0.342 g of $SbCl_3$ (5 at% to Sn), 4.6 ml HCl (37%), and DI water were mixed to homogeneity. Then an aqueous solution of NaOH (6 g in 100 ml DI water) was added. The total volume of the mixed solution was 150 ml. White precipitates were observed. The solution was moved to a three-necked flask and refluxed at 100 °C for 2 h in inert atmosphere. The color of the solution changed slowly to yellow during reflux. After refluxing, the solution was cooled, centrifuged, and evaporated. The dark-yellow solid thus obtained was heated in a tube furnace at 400 °C for 1 h in ambient air. The color of the ATO nanoparticles changed to bluish-gray after the heat treatment.

Preparation of Pt/ATO nanoparticles was based on the polyol method [21]. 0.8 g of $H_2PtCl_6{\cdot}xH_2O$ was dissolved in 200 ml of ethylene glycol containing 0.1 M NaOH. Next, the solution was refluxed in a three-necked flask at 160 °C for 30 min in inert atmosphere. Adequate amounts of the resultant Pt colloid were mixed with aqueous solutions of ATO nanoparticles. After stirring for several hours, 2 M H_2SO_4 was added to reduce the pH of the solutions. The solutions were filtered and evaporated. Finally, the electrocatalysts thus obtained were heated in a tube furnace at 160 °C for 2 h in air ambient to eliminate remaining organic materials. The nominal Pt content in the prepared electrocatalysts was 5, 10, 20, and 40 wt% to ATO. To compare the characteristics of electrocatalysts, 40 wt% Pt/C catalyst was prepared through the same procedure using Vulcan XC-72.

2.2. Catalyst characterization

Analysis of X-ray diffraction (XRD) was performed with Rigaku D/MAX 2500 operated with a CuK_α source ($\lambda = 1.541$ Å) at 40 kV and 100 mA with a scan rate of 2°/min. The electrical conductivities of antimony-doped and undoped SnO_2 nanoparticles were measured using the Van der Pauw configuration [22] with an Autolab (Eco Chemie) and a Keithley 2001 (Keithley instruments). Samples were prepared by creating round, 1.2-cm-diameter pellets. The specific surface areas of the electrocatalyst supports were calculated by a multipoint Brunauer–Emmett–Teller (BET) analysis of the nitrogen adsorption isotherms recorded on a surface area analyzer (Micromeritics ASAP 2020). Samples for transmission electron microscopy (TEM) were prepared by placing a drop of the particle-dispersed solution onto a carbon-coated copper grid and were examined using a JEOL 2010 TEM operated at 200 kV. X-ray photoelectron spectroscopy (XPS) was performed using an AXIS (Kratos) photoelectron spectrometer. The X-ray source was Mg$K\alpha$ operating at 15 kV and 150 W. Samples were prepared by depositing the electrocatalysts on a Si wafer using double-sided tape. TGA measurements were conducted in a thermal analyzer (SDT Q-600, TA Instruments) in the temperature range 25–800 °C at a heating rate of 3 °C/min in air flow (50 ml/min) using an alumina sample pan.

2.3. Electrochemical measurements

Cyclic voltammograms were obtained in a conventional three-electrode electrochemical cell using glassy carbon electrode (6 mm diameter) as a working electrode, platinum wire as a counter-electrode, and saturated calomel electrode (SCE) as a reference electrode. Electrochemical measurements were all recorded and reported versus normal hydrogen electrode (NHE). The glassy carbon electrode was polished with 1-, 0.3-, and 0.05-μm Al_2O_3 slurries and washed ultrasonically with DI water before use. Inks were prepared by mixing prepared electrocatalysts, DI water, 2-propanol (Junsei), and a 5 wt% Nafion solution (Aldrich) as a binding material. For the Pt/ATO (Pt/C) electrocatalysts, the inks were prepared by adding the following amounts of each solution per 0.1 g of the catalyst: 60 μl (200 μl) of DI water, 150 μl (500 μl) of Nafion solution, and 2 ml (5 ml) of 2-propanol. The inks were dropped onto glassy carbon (GC) electrodes with a micropipette, and the carbon electrodes were then dried in a vacuum oven. Electrochemical experiments were performed with an Eco Chemie Autolab. Solutions of 0.5 M H_2SO_4, 0.5 M H_2SO_4/1 M CH_3OH, and 0.5 M H_2SO_4/1 M C_2H_5OH were purged with nitrogen gas before the measurements. To identify the activities of the electrocatalysts, voltammetry was conducted in the potential between 0.05 and 1.2 V versus NHE at a scan rate of 20 mV/s. Chronoamperometry was performed in 0.5 M H_2SO_4/1 M CH_3OH and 0.5 M H_2SO_4/1 M C_2H_5OH for 2 h. CO-stripping voltammetry was performed in the same potential range. CO molecules were adsorbed on the electrocatalysts at a potential of 0.1 V versus NHE by bubbling 0.5 M H_2SO_4 with 10% CO/He gas for 20 min; the dissolved CO gas in the solution was then removed by bubbling with Ar gas for 30 min. To investigate the electrochemical stabilities of the prepared electrocatalysts, potential cycling was conducted up to 1000 cycles in 0.5 M H_2SO_4 with a scan rate of 50 mV/s. The solutions were bubbled with Ar gas during potential cycling.

3. Results and discussion

3.1. Structural characterization

The synthesized ATO nanoparticles and the Pt/ATO electrocatalysts were analyzed by XRD. The top diffractogram in Fig. 1 shows a typical polycrystalline diffraction of cassiterite SnO_2 [23]. No phase ascribed to Sb compounds can be seen, indicating that all Sb ions have substituted for Sn ions. The size of the ATO nanoparticles calculated from the (110) peak using Scherrer's equation was

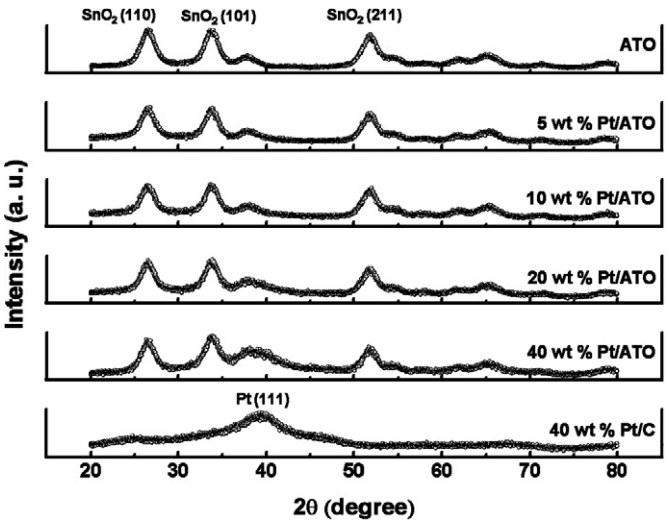

Fig. 1. XRD patterns of the ATO support and the prepared electrocatalysts.

Table 1
Results of BET analysis

	ATO	Vulcan XC-72
BET surface area (m^2/g)	99.7	239.6
Pore volume (cm^3/g)		
Total	0.12	0.32
BJH cumulative adsorption	0.128	0.406
BJH cumulative desorption	0.127	0.409
Pore size (nm)		
Average	4.77	5.26
BJH cumulative adsorption	4.02	10.46
BJH cumulative desorption	3.46	10.24

~5.2 nm. The effect of Sb doping could be proven by the measurement of electrical conductivities. The electrical conductivities of undoped and Sb-doped SnO_2 were 0.0028 and 0.11 S/cm, respectively. The specific surface areas of the ATO and the Vulcan XC-72R from a BET analysis were 99.7 and 239.6 m^2/g, respectively. The detailed results of BET analysis for pore sizes and pore volumes are collected in Table 1. The 40 wt% Pt/C electrocatalyst (bottom diffractograms in Fig. 1) exhibited a characteristic pattern of polycrystalline Pt diffraction. The diffraction peaks at around 39°, 46°, and 68° were due to diffractions at Pt (111), (200), and (220) planes, respectively. The pattern was too broad to be resolved, indicating very small Pt particles. Diffraction patterns for Pt/ATO electrocatalysts exhibited diffraction peaks from both ATO and Pt particles. As Pt-loading decreased, the diffraction peak of the Pt (111) plane diminished, whereas that of the ATO remained at the same intensity. The (101) diffraction of the ATO particles was distorted with increasing Pt loading; this can be attributed to the broad diffraction peak from the Pt (111) plane, as shown in the diffractogram of the Pt/C electrocatalyst.

TEM images were obtained to provide more information on the Pt particle size and particle distribution. Fig. 2 shows the TEM images of ATO nanoparticles and the prepared electrocatalysts. As shown in Figs. 2a and 2b, the ATO particles were uniform and spherical. In addition, the electron diffraction pattern (inset of Fig. 2a) showed good crystallinity of the ATO particles. The size of the ATO particles from TEM images was ~5 nm, in accordance with the XRD findings. Fig. 2c shows well-distributed Pt particles on carbon support. The average particle size from TEM was ~2.5 nm. It should be noted that all of the prepared electrocatalysts were synthesized using the same Pt colloid; therefore, the PT particles should have the same average size in all of the prepared electrocatalysts. Figs. 2d, 2e, and 2f show TEM images of the Pt/ATO electrocatalysts for the 40, 10, and 5 wt% Pt/ATO samples, respectively. As Pt loading decreased, the distribution of Pt particles on the ATO support became remarkable. In the 40 wt% Pt/ATO sample, Pt particles covered most of the ATO surface and were stacked on top of one another; whereas in the 5 wt% Pt/ATO sample, the Pt particles were evenly distributed on the ATO surface.

Table 2 gives the binding energies (BEs) of Pt $4f_{7/2}$ and Sn $3d_{5/2}$ from the XPS spectra. The BE of metallic Pt in Pt/C was slightly shifted from the value of bulk Pt (70.9 eV) to higher energy, due to the small size of Pt particles or to the interaction between Pt particles and the carbon support [24]. For the Pt/ATO, the BE of metallic Pt shifted to slightly lower energy. Similar results have been reported previously [24,25]. The observed negative shift in the BE may be attributed to the electron transfer from Sn to Pt [24]. Small amounts of Pt and Sn atoms may have interdiffused to form Pt–Sn or Pt–Sn–O complexes at the Pt–ATO interface during heat treatment; however, the negative shift in the BE was too small to allow us to draw this conclusion. At this stage, the effect of the BE shift was uncertain, and this merits further investigation.

3.2. Electrochemical characterizations

Fig. 3 shows the cyclic voltammograms for 0.5 M H_2SO_4. All of the samples exhibited H-adsorption/desorption peaks at 0.05–0.3 V and Pt-oxide formation/reduction peaks at ~0.9/0.75 V. The anodic peak at ~0.7 V indicates the oxidation of a Sn–O species, which was not seen in the Pt/C sample. As Pt loading decreased, the double-layer capacitance increased gradually. This means that the charge transfer in the 40 wt% Pt/ATO sample occurred mainly on the Pt surface, whereas that in the 5 wt% Pt/ATO sample occurred not only on the Pt surface, but also on the ATO surface. This was expected, based on the TEM images shown in Fig. 2.

Figs. 4a and 4b show the CO-stripping voltammograms and the electrochemical active surface areas (ESAs) defined by the H-desorption area and the CO-stripping area of the samples. The CO-stripping voltammograms of the Pt/ATO samples were very broad, indicating that the Pt/ATO electrocatalysts contained various states of active sites. The peak at 0.4 V, the so-called "pre-peak," has been attributed to the electrooxidation of weakly adsorbed CO, whereas the main peak at 0.7–0.8 V has been attributed to that of strongly adsorbed CO [26,27]. The pre-peak was hardly observed in the Pt/C, but was clearly seen in the Pt/ATO. The main peaks of the Pt/ATO were shifted negatively by ~0.1 V compared with that of the Pt/C. This indicates that the Pt/ATO electrocatalysts were more effective than the Pt/C electrocatalyst for electrooxidation of both weakly and strongly adsorbed CO. Moreover, the onset potentials of CO oxidation for Pt/ATO were <0.3 V, which are negative by ~0.3 V compared with those for Pt/C, and the onset potentials became less positive as the amount of Pt-loading decreased. This indicates that the prepared Pt/ATO electrocatalysts are highly CO-tolerant. Arentz et al. [28] proposed that SnO_2 adjacent to Pt may provide a bifunctional effect in the following steps:

$$Pt + CO_{diss} = Pt\text{–}CO_{ad},$$
$$SnO_2 + H_2O = SnO_2\text{–}OH_{ad} + H^+ + e^-,$$
$$Pt\text{-}CO_{ad} + SnO_2\text{–}OH_{ad} = CO_2 + H^+ + e^-.$$

Santos et al. [12] suggested that the bifunctional effect and the electronic effect may coexist in Pt electrocatalysts supported on SnO_2. The ESAs calculated from H-desorption and CO-stripping were close to one another. The Pt/ATO samples had lower ESAs than the Pt/C sample due to the lower surface area of ATO, as mentioned in Section 3.1. The ESAs of the Pt/ATO samples increased with decreasing Pt loading, indicating better dispersion of Pt particles on the ATO support.

3.3. Alcohol oxidation

The electrooxidation of methanol on the prepared electrocatalysts was performed using cyclic voltammetry. Fig. 5 shows the results at 0.6 V as well as the entire curves. The oxidation current normalized by the Pt mass (mass specific activity) was proportional to the specific activity of active sites and catalyst dispersion on the support; in contrast, the oxidation current normalized by the ESA (i.e., surface specific activity) was proportional only to the specific activity of the active sites. The mass specific activity of the Pt/ATO samples for MOR increased with decreasing Pt loading due to the higher ESAs and increased CO tolerance. In addition, the mass specific activity of the Pt/ATO samples was higher than that of the Pt/C catalyst, with the exception of the 40 wt% Pt/ATO sample. This is most likely due to enhancement of the surface specific activity, which in turn may be related to the greater CO tolerance. As the ESA of the Pt/ATO electrocatalyst increased, the portion of Pt particles adjacent to ATO also increased, because higher ESA means better dispersion of Pt particles. Consequently, the bifunctional effect and/or the electronic effect also increased.

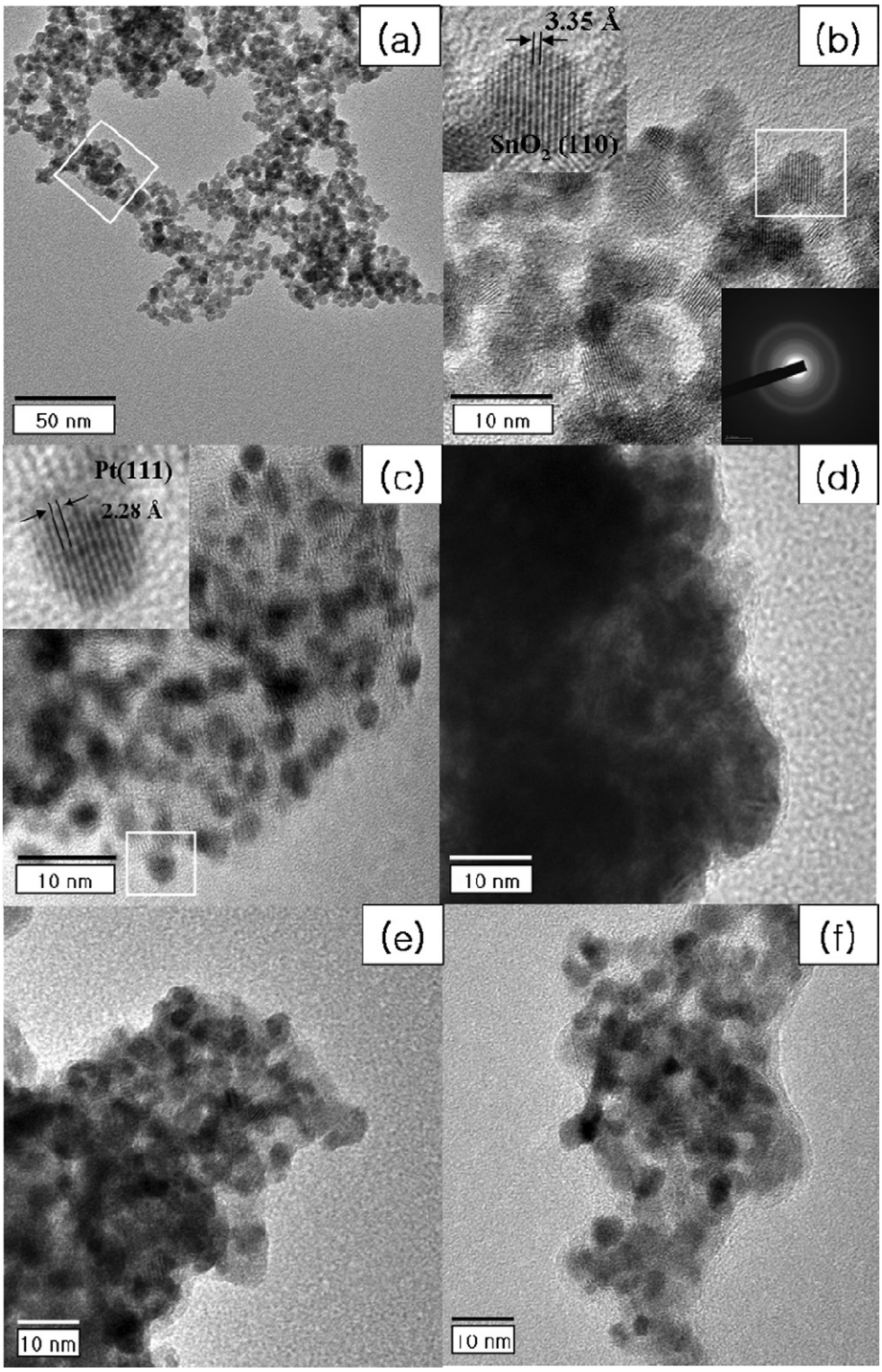

Fig. 2. TEM images of (a) ATO, (b) magnified one of (a), (c) 40 wt% Pt/C, (d) 40 wt% Pt/ATO, (e) 10 wt% Pt/ATO, and (f) 5 wt% Pt/ATO.

Table 2
Binding energy of the prepared electrocatalysts from Pt $4f_{7/2}$ and Sn $3d_{5/2}$ photoelectron spectra

Electrocatalysts	Binding energy (eV)			
	Pt^0	Pt^{2+}	Pt^{4+}	Sn^{4+}
5 wt% Pt/ATO	70.84	72.2	73.9	486.82
20 wt% Pt/ATO	70.99	72.3	73.75	486.99
40 wt% Pt/ATO	71.24	72.48	74.11	486.97
40 wt% Pt/C	71.15	72.4	74.0	

Repeated CVs for MOR on the 40 wt% Pt/C and 5 wt% Pt/ATO were performed for up to 100 cycles with a scan rate of 50 mV/s, to investigate sample stability in the presence of fuel. The results of the 5th and every 10th cycling were recorded and are shown in Fig. 5d. The current decrease on Pt/ATO was slow and almost constant after 70 cycles, whereas that on Pt/C was still decreasing at 100 cycles, indicating that the Pt/ATO was more stable than the Pt/C for MOR.

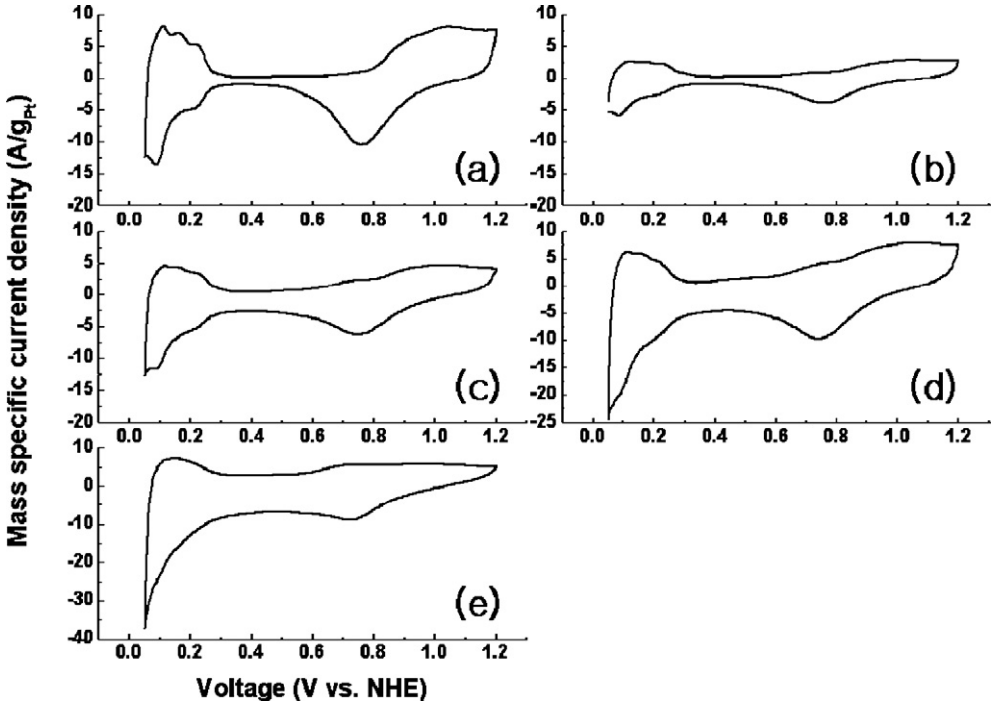

Fig. 3. Cyclic voltammograms of (a) 40 wt% Pt/C, (b) 40 wt% Pt/ATO, (c) 20 wt% Pt/ATO, (d) 10 wt% Pt/ATO, and (e) 5 wt% Pt/ATO.

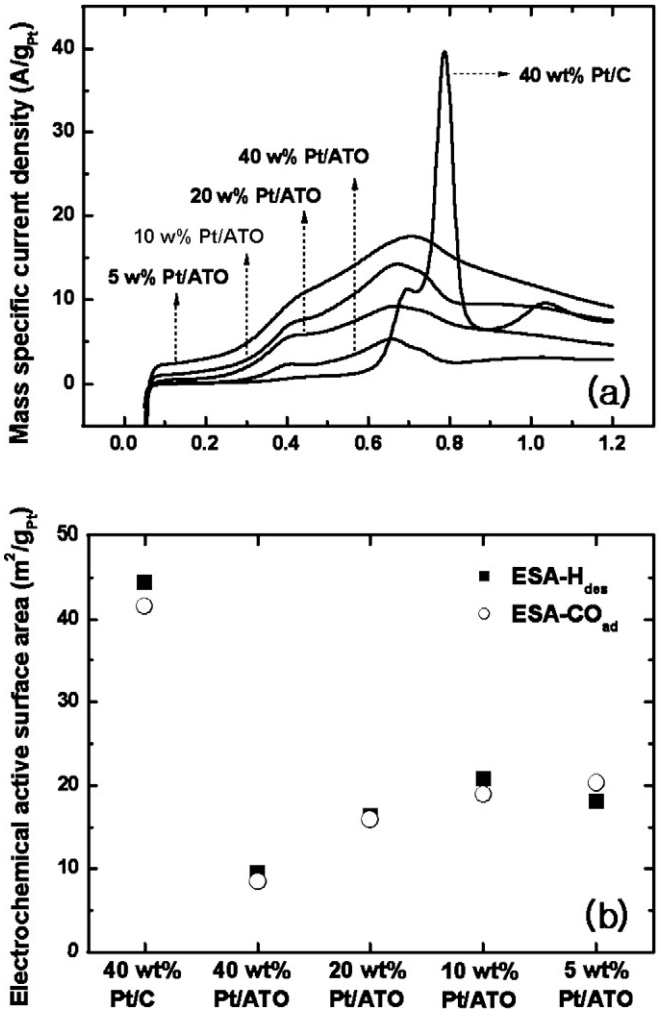

Fig. 4. (a) Anodic parts of the CO-stripping voltammogram. (b) ESAs calculated from the hydrogen desorption area (■) and CO-stripping area (○).

Fig. 6 shows the results of ethanol electrooxidation using CV. All of the Pt/ATO samples exhibited higher mass specific activity and surface specific activity for EOR compared with the Pt/C sample. The roles of SnO_2 in the Pt-based catalyst for EOR include supplying OH species at low potential for the oxidation of CO_{ad} and slightly changing the lattice constant of Pt for easier adsorption of ethanol or C–C bond cleavage [12,28–32]. These two effects also may be applicable to the Pt/ATO samples. The first role of SnO_2 was confirmed by CO-stripping voltammetry, as shown in Fig. 4a; however, the second role was uncertain in the present experiment, because of the unclear position of the XRD peak of Pt (111) caused by superpositioning on SnO_2 (200) diffraction.

The EOR activity of the Pt/ATO was enhanced over that of the Pt/C to a much greater degree than the MOR activity. Compared with the Pt/C catalyst (at 0.6 V), the EOR activity of the 5 wt% Pt/ATO was increased 6-fold for the mass specific activity and 13-fold for the surface specific activity, whereas the MOR activity was enhanced 1.6-fold for the mass specific activity and 2.3-fold for the surface specific activity. This significant difference can be attributed to the more suitable electronic states of Pt or to differing properties for adsorption of methanol or ethanol [33].

Fig. 6d shows the normalized current at 0.6 V in repeated CV for EOR on the 40 wt% Pt/C and 5 wt% Pt/ATO. The current decrease was slower on Pt/ATO than on Pt/C, indicating that the Pt/ATO was more stable than the Pt/C for both MOR and EOR in the presence of fuels.

The ratio of forward (I_f) and backward (I_b) peak current can be used to describe the CO tolerance of catalysts [34,35]. High I_f/I_b values imply high CO tolerance. The I_f/I_b value of Pt/C was ~0.6, whereas that of 5, 10, and 20 wt% Pt/ATO was 0.8–0.9. Table 3 gives the forward (P_f) and backward (P_b) peak potentials of the samples for both MOR and EOR. The forward and backward peak potentials shifted to lower potentials as Pt loading decreased over those of Pt/C. At peak potentials of alcohol oxidation, OH adsorbed on Pt inhibits fuel adsorption to decrease the oxidation current [36]. If the OH supply is promoted by a bifunctional effect, then the peak potentials should appear at lower potentials. Therefore,

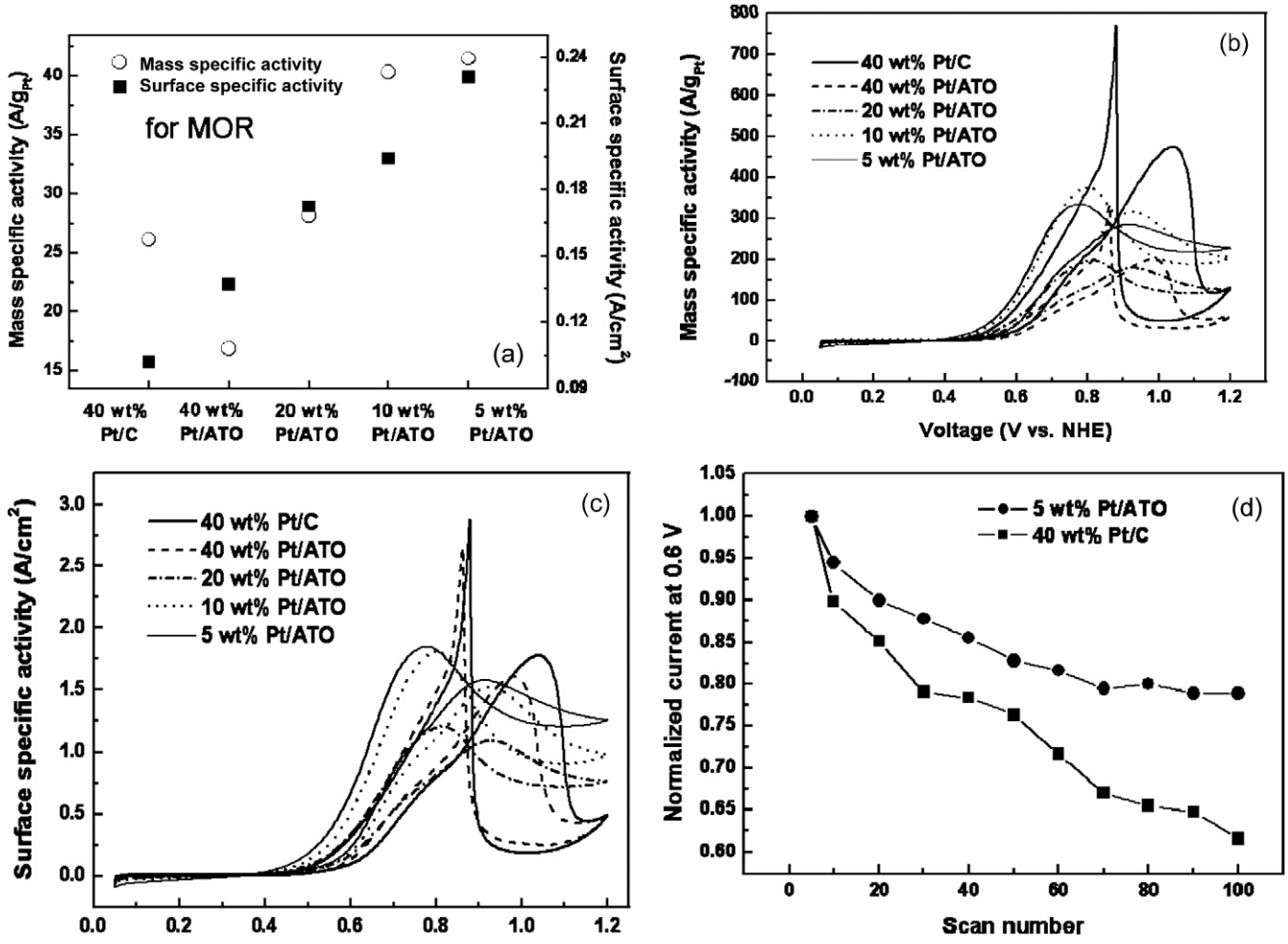

Fig. 5. (a) Mass (○)- and surface (■)-normalized MOR activities of the electrocatalysts at 0.6 V vs NHE. (b) Mass- and (c) surface-normalized cyclic voltammetry, (d) normalized current at 0.6 V in repeated CV for MOR on 5 wt% Pt/ATO (●) and on 40 wt% Pt/C (■).

higher I_f/I_b values and lower peak potentials of Pt/ATO in alcohol oxidation closely match the results of CO oxidation.

As was mentioned in Section 3.1, the electrical conductivity of ATO was 0.11 S/cm, which is lower than that of carbon (Vulcan XC-72) by ∼1 order. Electrocatalytic activities of catalysts are affected by active surface area, electrical conductivities, and intrinsic activities. The surface specific activities were higher for the Pt/ATO samples compared with Pt/C; this means that the positive effect (i.e., higher intrinsic activities of Pt/ATO) exceeded the negative effect (i.e., lower electrical conductivity of ATO). Up to now, the extent to which the electrical conductivity of the support material affects electrocatalytic activity has been unknown. But higher electrocatalytic activity for the oxygen reduction reaction using an Nb-doped TiO_2 support compared with that using a carbon support has been reported [37], where the electrical conductivity of Nb-doped TiO_2 was found to be similar to that of ATO. In addition, our group reported work on a support material using conducting polymers [38], in which the electrical conductivity of the polymer (P4VPCz) was lower by several orders of magnitude (nearly $\sim 10^{-10}$ S/cm) than that of Vulcan XC-72. However, the unit cell performance of PtRu/P4VPCz (maximum power density of 152 mW) was comparable to that of PtRu/C (maximum power density of 171 mW). Based on those findings, the higher electrocatalytic activity of the Pt/ATO samples compared with Pt/C reported here are reasonable.

Chronoamperometry for MOR and EOR were performed on the Pt/ATO samples (5 and 10 wt%) at 0.5 V for 2 h, and the resulting activities were compared with those of Pt/C, PtRu/C (E-tek), and 5 wt% Pt/SnO_2 (5 wt% Pt/TO). As shown in Fig. 7a, the mass specific current densities for MOR of the Pt/ATO samples were higher than that of Pt/C but lower than that of PtRu/C. The 5 wt% Pt/ATO sample exhibited higher current density than the 5 wt% Pt/TO sample, again confirming the Sb-doping effect. Interestingly, the 5 wt% Pt/TO exhibited a higher current density than Pt/C, despite a much lower electrical conductivity (by ∼3 orders) of SnO_2 than that of carbon, clearly demonstrating the effect of SnO_2 as a promoting support. In contrast, the electrical conductivity of the support material had no significant affect. The EOR activities of the Pt/ATO were enhanced over those of Pt/C and PtRu/C to a much greater degree than the MOR activities. These findings correspond to those of CV.

3.4. Electrochemical stability

The electrochemical stabilities of the prepared samples were investigated using potential cycling up to 1000 cycles in 0.5 M H_2SO_4 at 40 °C. Potential cycling causes dissolution of Pt during the anodic portions of the cycles or during the reduction of Pt oxides [39]. Some of the dissolved Pt moves into the electrolyte solution, and some may be redeposited onto Pt particles. The dissolved Pt can be reduced electrochemically and may diffuse to be redeposited on a larger particle, thereby increasing the particle size. At the same time, carbon corrosion can occur, accelerating particle growth on the carbon support. In the presence of Pt on the carbon

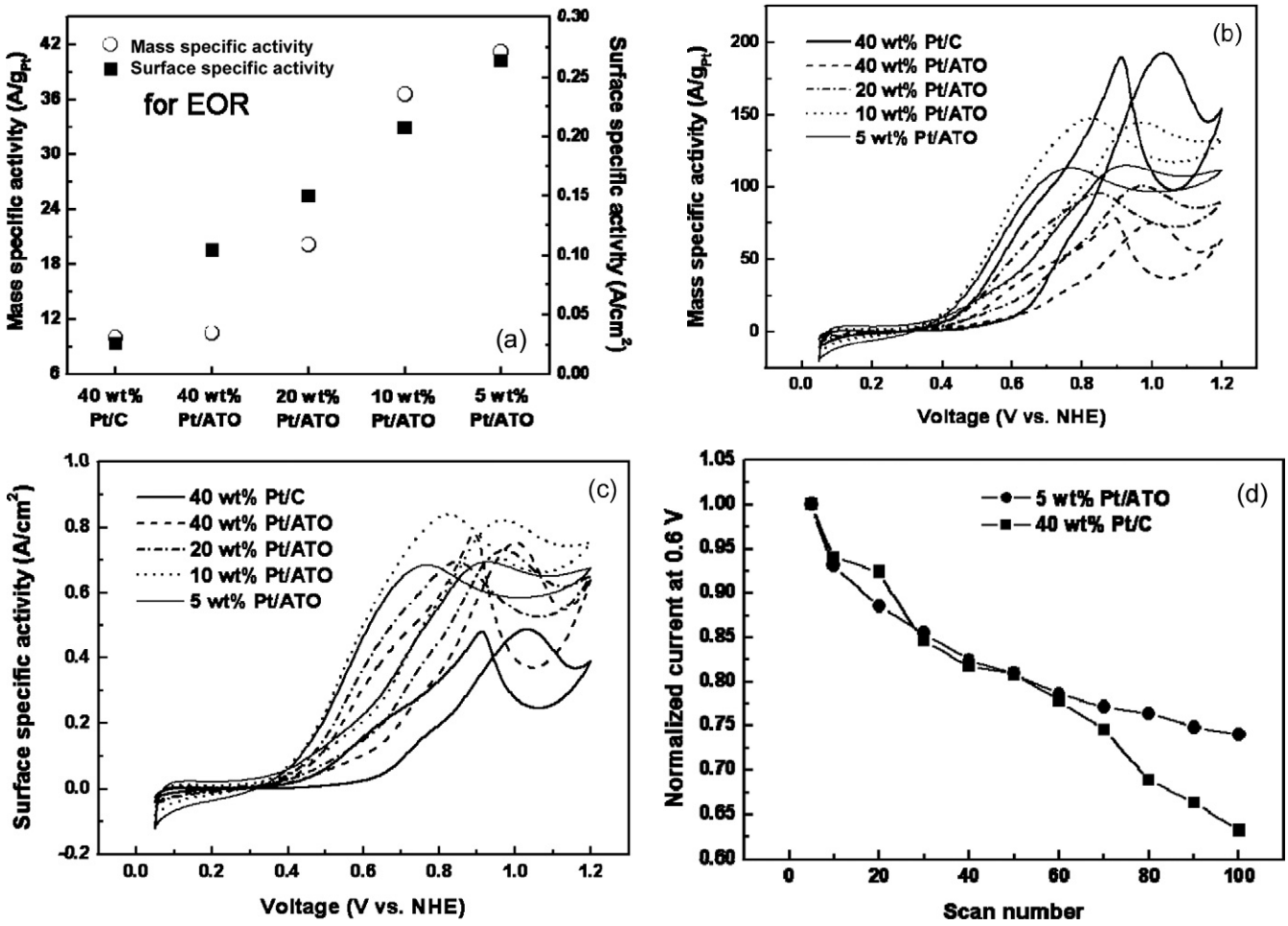

Fig. 6. (a) Mass (○)- and surface (■)-normalized EOR activities of the electrocatalysts at 0.6 V vs NHE. (b) Mass- and (c) surface-normalized cyclic voltammetry, (d) normalized current at 0.6 V in repeated CV for EOR on 5 wt% Pt/ATO (●) and on 40 wt% Pt/C (■).

Table 3
Forward (P_f) and backward (P_b) peak potentials of cyclic voltammograms for MOR and EOR

Peak potentials (V)	5 wt% Pt/ATO	10 wt% Pt/ATO	20 wt% Pt/ATO	40 wt% Pt/ATO	40 wt% Pt/C
MOR-P_f	0.9	0.92	0.93	0.98	1.04
MOR-P_b	0.77	0.8	0.81	0.86	0.88
EOR-P_f	0.92	0.96	0.97	1	1.03
EOR-P_b	0.76	0.82	0.84	0.89	0.91

support, OH species adsorbed on Pt can oxidize the carbon support, forming gaseous carbon dioxide [17,18]. Eventually, catalyst particles can agglomerate, causing a decrease in the active surface area of the catalyst.

In the present experiment, the normalized surface areas were calculated from H_{des} charge during potential cycling; these are shown in Fig. 8. All of the samples exhibited a gradual decline in surface area with repeated potential cycling, probably due to dissolution of Pt and the growth of Pt particles [17,39–41]. For the Pt/C sample, the initial cycles increased the surface area, most likely due to electrochemical cleaning of the Pt surface [17,42]. But this initial increase was not seen for the Pt/ATO samples, likely due to the different surface states and amounts of impurities on the support material [17]. The total area loss in the Pt/C sample was about 60%. The area loss was ∼30% in the 5 wt% Pt/ATO and ∼40% in the 20 wt% Pt/ATO, indicating that the Pt/ATO samples were much more electrochemically stable than the Pt/C sample. The smaller area loss for the Pt/ATO catalysts during potential cycling can be attributed to the corrosion resistance of ATO [20]. The greater corrosion resistance of the Pt/ATO over the Pt/C in an oxidative environment was demonstrated by TGA, as shown in Fig. 9. The normalized weight loss was approximately 60% for the Pt/C, compared with about 4% for the Pt/ATO. Most of the weight loss for the Pt/C occurred at about 400 °C, due to Pt-catalyzed oxidation of the carbon support [18,20]. The thermogravimetric property of the Pt/ATO catalyst indicates that the ATO support was stable in the oxidative environment; this stability can be related to the electrochemical stability of the Pt/ATO catalysts [18,20].

Another possible reason for the electrochemical stability of the Pt/ATO samples may be the strong interaction between the ATO support and the Pt atoms or clusters redeposited after the electrochemical dissolution. The carbon support has a smooth surface and only weakly interacts with metals; thus, the Pt redeposited after the electrochemical dissolution can readily diffuse to form large Pt particles. In contrast, oxide supports have rough surfaces and strongly interact with metals. As a result, oxide supports can anchor the redeposited Pt and suppress the growth of Pt particles. Nagai et al. [43] investigated the interactions between Pt and ceria-based oxides and sintering inhibition mechanisms through sintering experiments in oxidizing atmospheres. They attributed the sintering inhibition effect to the formation of Pt–O–Ce bond, which can act as an anchor and thereby inhibit Pt migration. Shih and Chang [44] prepared TiO_2 grafted on carbon and carbon-supported Pt catalysts and studied catalyst deactivation at high temperatures (>130 °C). They concluded that the TiO_2 was able to anchor Pt particles by interacting with Pt, thereby inhibiting Pt migration and

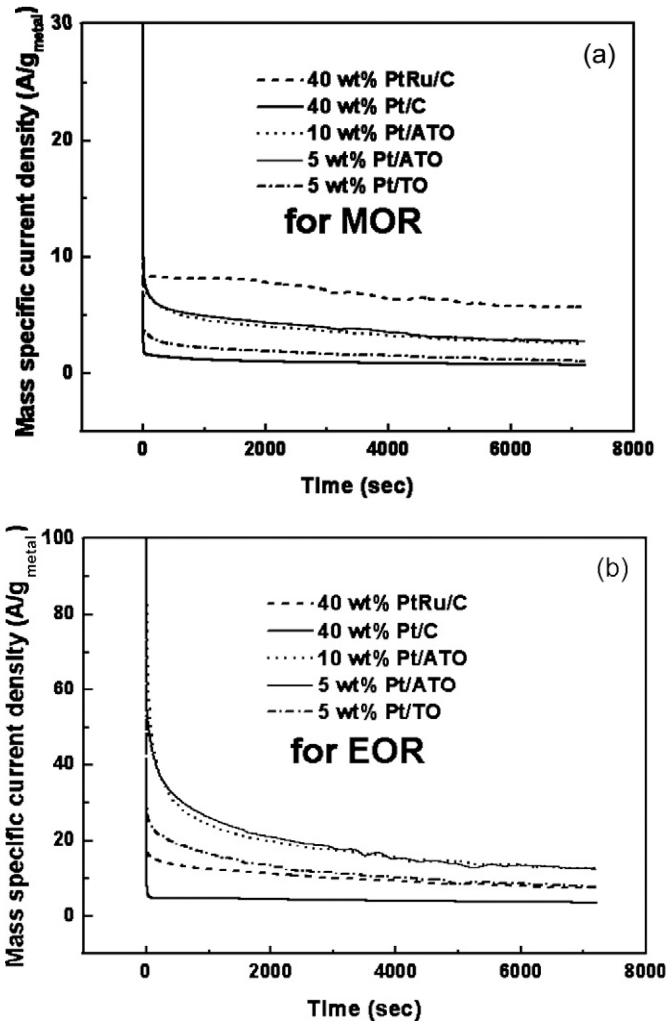

Fig. 7. Chronoamperometry diagrams for (a) MOR and (b) EOR measured at 0.5 V vs NHE for 30 min.

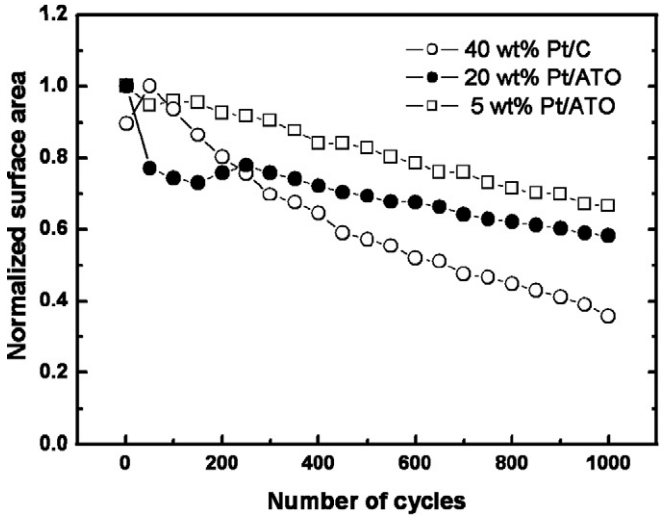

Fig. 8. Normalized H_{des} areas of 40 wt% Pt/C (○), 20 wt% (●), and 5 wt% (□) Pt/ATO during potential cycling.

agglomeration. Although the degree of interaction between Pt and oxide supports may not be the same, the foregoing mechanism may be applicable to the Pt/ATO samples as well.

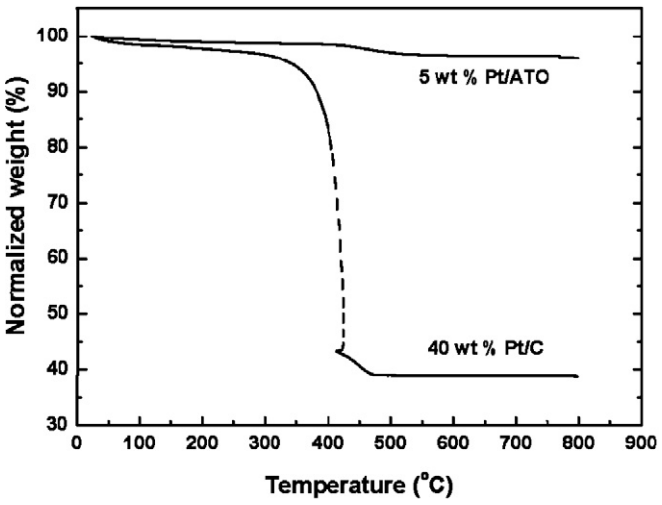

Fig. 9. TGA data for 40 wt% Pt/C and 5 wt% Pt/ATO.

Fig. 10 presents TEM images of the 40 wt% Pt/C and the 5 wt% Pt/ATO after the potential cycling. Fig. 10a clearly shows the increased size of the Pt particles. Before the potential cycling, the particle size on the carbon support was 2–3 nm, with a narrow size distribution, as mentioned in Section 3.2. After the potential cycling, the distribution of particle size was >10 nm. But the particle growth in the Pt/ATO was not significant compared with that in the Pt/C, as shown in Fig. 10b. The representative high-magnification images of 5 wt% Pt/ATO before and after potential cycling presented in Figs. 10c–10f show 2–3 nm Pt particles before potential cycling and mostly <5 nm Pt particles after potential cycling. Although the size of the Pt particles is not clear in the low-magnification image (Fig. 10b), the lower growth rate of Pt particles in 5 wt% Pt/ATO sample is confirmed by the high-magnification images. Therefore, the electrochemical stability of the Pt/ATO electrocatalysts must be attributed to the slower rate of particle growth.

4. Conclusion

In this work, Pt/ATO electrocatalysts were prepared with various amounts of Pt loaded on ATO. The electrochemical activities of the Pt/ATO for CO oxidation, MOR, and EOR were compared with those of the Pt/C. The Pt/ATO electrocatalysts were highly CO-tolerant. The activities of the Pt/ATO for both MOR and EOR were greater than those of the Pt/C as the amount of loaded Pt decreased. These enhanced activities can be attributed to better dispersion of Pt particles on the ATO support, as well as to the effects of SnO_2 adjacent to Pt, such as the bifunctional effect and/or the electronic effect. In addition, significant differences in the enhancement of MOR and EOR activities we seen. The stabilities of the prepared electrocatalysts were investigated using potential cycling, TGA, and TEM. The Pt/ATO exhibited much higher stabilities than the Pt/C, which can be attributed to higher corrosion resistance of the ATO support and the strong interaction between Pt redeposited after electrochemical dissolution and the ATO support. The slower growth rate of Pt particles on the ATO support was apparent from the TEM images obtained after the potential cycling.

For practical applications, the synthesis of ATO support needs to be improved to achieve higher surface areas, higher electrical conductivities, and appropriate pore sizes. Based on the results of this study, the ATO nanoparticle appears to be a promising material as an active and stable support for DAFCs.

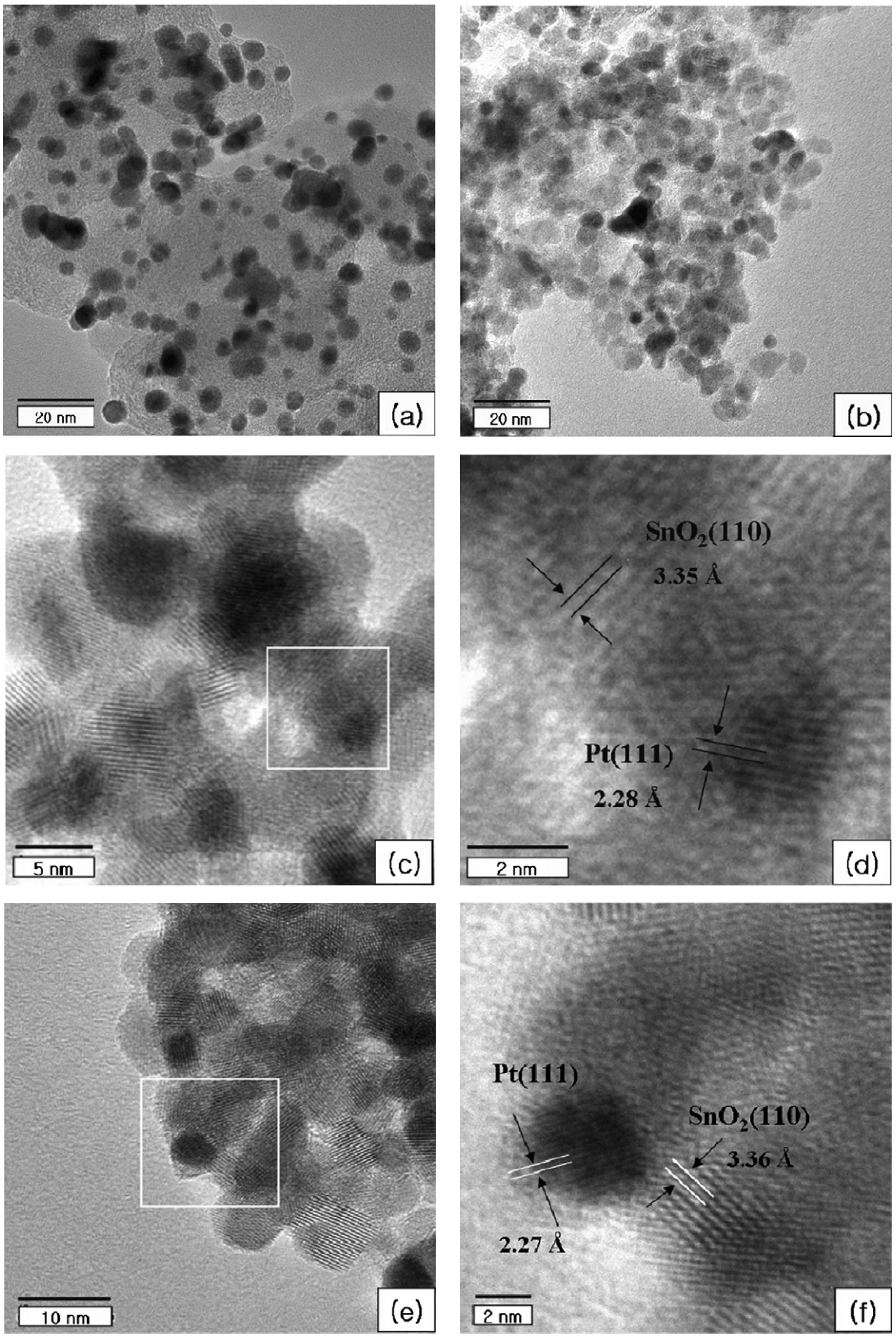

Fig. 10. TEM images taken after potential cycling for 40 wt% Pt/C (a) and 5 wt% Pt/ATO (b), magnified images taken before (c and d) and after (e and f) potential cycling for 5 wt% Pt/ATO.

Acknowledgments

This work was supported by the Ministry of Commerce, Industry and Energy through the Research Center for Energy Conversion and Storage and the Korea Research Foundation (Grant KRF-2006-005-J04601).

References

[1] K.-Y. Chan, J. Ding, J. Ren, S. Cheng, K.Y. Tsang, J. Mater. Chem. 14 (2004) 505.
[2] W. Zhou, Z. Zhou, S. Song, W. Li, G. Sun, P. Tsiakaras, Q. Xin, Appl. Catal. B 46 (2003) 273.
[3] K.-W. Park, J.-H. Choi, S.-A. Lee, C. Pak, H. Chang, Y.-E. Sung, J. Catal. 224 (2004) 236.
[4] T. Kawaguchi, W. Sugimoto, Y. Murakami, Y. Takasu, J. Catal. 229 (2005) 176.
[5] I.-S. Park, B. Choi, D.-S. Jung, Y.-E. Sung, Electrochim. Acta 52 (2006) 1683.
[6] S.-A. Lee, K.-W. Park, B.-K. Kwon, Y.-E. Sung, J. Ind. Eng. Chem. 9 (2003) 63.
[7] K.-W. Park, Y.-E. Sung, S. Han, Y. Yun, T. Hyeon, J. Phys. Chem. B 108 (2004) 939.
[8] I.-S. Park, K.-W. Park, J.-H. Choi, C.R. Park, Y.-E. Sung, Carbon 45 (2007) 28.
[9] A.C.C. Tseung, K.Y. Chen, Catal. Today 38 (1997) 439.
[10] B.L. Garcia, R. Fuentes, J.W. Weidner, Electrochem. Solid State Lett. B 10 (2007) 108.
[11] B. Moreno, E. Chinarro, J.L.G. Fierro, J.R. Jurado, J. Power Sources 169 (2007) 98.
[12] A.L. Santos, D. Profeti, P. Olivi, Electrochim. Acta 50 (2005) 2615.
[13] K.-W. Park, Y.-E. Sung, J. Ind. Eng. Chem. 12 (2006) 165.
[14] T. Okanishi, T. Matsui, T. Takeguchi, R. Kikuchi, K. Eguchi, Appl. Catal. A 298 (2006) 181.
[15] L. Jiang, G. Sun, Z. Zhou, S. Sun, Q. Wang, S. Yan, H. Li, J. Guo, B. Zhou, Q. Xin, J. Phys. Chem. B 109 (2005) 8774.
[16] K. Kinoshita, Carbon: Electrochemical and Physicochemical Properties, Wiley, New York, 1988, p. 319.
[17] B. Merzougui, S. Swathirajan, J. Electrochem. Soc. A 153 (2006) 2220.
[18] M. Cai, M.S. Ruthkosky, B. Merzougui, S. Swathirajan, M.P. Balogh, S.H. Oh, J. Power Sources 160 (2006) 977.
[19] T. Ioroi, Z. Siroma, N. Fujiwara, S. Yamazaki, K. Yasuda, Electrochem. Commun. 7 (2005) 183.
[20] H. Chhina, S. Campbell, O. Kesler, J. Power Sources 161 (2006) 893.
[21] C. Bock, C. Paquet, M. Couillard, G.A. Botton, B.R. MacDougall, J. Am. Chem. Soc. 126 (2004) 8028.
[22] D.K. Schroder, Semiconductor Material and Device Characterization, Wiley, New York, 1998, p. 14.
[23] H.-J. Ahn, H.-C. Choi, K.-W. Park, S.-B. Kim, Y.-E. Sung, J. Phys. Chem. B 108 (2004) 9815.
[24] A.K. Shukla, A.S. Arico, K.M. El-Khatib, H. Kim, P.L. Antonucci, V. Antonucci, Appl. Surf. Sci. 137 (1999) 20.
[25] K. Ke, K. Waki, J. Electrochem. Soc. A 154 (2007) 207.
[26] E.M. Crabb, R. Marshall, D. Thompsett, J. Electrochem. Soc. 147 (2000) 4440.
[27] Y. Morimoto, E.B. Yeager, J. Electroanal. Chem. 441 (1998) 77.
[28] M. Arenz, V. Stamenkovic, B.B. Blizanac, K.J. Mayrhofer, N.M. Markovic, P.N. Ross, J. Catal. 232 (2005) 402.
[29] L. Jiang, G. Sun, S. Sun, J. Liu, S. Tang, H. Li, B. Zhou, Q. Xin, Electrochim. Acta 50 (2005) 5384.
[30] L. Jiang, L. Colmenares, Z. Jusys, G.Q. Sun, R.J. Behm, Electrochim. Acta 53 (2007) 377.
[31] H. Li, G. Sun, L. Cao, L. Jiang, Q. Xin, Electrochim. Acta 52 (2007) 6622.
[32] W.J. Zhou, S.Q. Song, W.Z. Li, Z.H. Zhou, G.Q. Sun, Q. Xin, S. Douvartzides, P. Tsiakaras, J. Power Sources 140 (2005) 50.
[33] A.O. Neto, R.R. Dias, M.M. Tusi, M. Linardi, E.V. Spinacé, J. Power Sources 166 (2007) 87.
[34] Z. Liu, X.Y. Ling, X. Su, J.Y. Lee, J. Phys. Chem. B 108 (2004) 8234.
[35] Y. Lin, X. Cui, Langmuir 21 (2005) 11474.
[36] A. Hamnett, Catal. Today 38 (1997) 445.
[37] K.-W. Park, K.-S. Seol, Electrochem. Commun. 9 (2007) 2256.
[38] J.-H. Choi, K.-W. Park, H.-K. Lee, Y.-M. Kim, J.-S. Lee, Y.-E. Sung, Electrochim. Acta 48 (2003) 2781.
[39] K.-I. Ota, S. Nishigori, N. Kamiya, J. Electroanal. Chem. 257 (1988) 205.
[40] K. Kinoshita, J.T. Lundquist, P. Stonehart, J. Electroanal. Chem. 48 (1973) 157.
[41] X. Wang, R. Kumar, D.J. Myers, Electrochem. Solid State Lett. A 9 (2006) 225.
[42] M.W. Breiter, Electrochim. Acta 11 (1966) 905.
[43] Y. Nagai, T. Hirabayashi, K. Dohmae, N. Takagi, T. Minami, H. Shinjoh, S. Matsumoto, J. Catal. 242 (2006) 103.
[44] C.-C. Shih, J.-R. Chang, J. Catal. 240 (2006) 137.